Editors' Suggestion | Featured in Physics

Ponderomotive Squeezing of Light by a Levitated Nanoparticle in Free Space

Andrei Militaru,[1] Massimiliano Rossi,[1] Felix Tebbenjohanns,[1,*] Oriol Romero-Isart,[2,3] Martin Frimmer,[1] and Lukas Novotny[1,4]

[1]*Photonics Laboratory, ETH Zürich, CH-8093 Zürich, Switzerland*
[2]*Institute for Quantum Optics and Quantum Information of the Austrian Academy of Sciences, A-6020 Innsbruck, Austria*
[3]*Institute for Theoretical Physics, University of Innsbruck, A-6020 Innsbruck, Austria*
[4]*Quantum Center, ETH Zürich, CH-8093 Zürich, Switzerland*

(Received 19 February 2022; accepted 14 June 2022; published 25 July 2022)

A mechanically compliant element can be set into motion by the interaction with light. In turn, this light-driven motion can give rise to ponderomotive correlations in the electromagnetic field. In optomechanical systems, cavities are often employed to enhance these correlations up to the point where they generate quantum squeezing of light. In free-space scenarios, where no cavity is used, observation of squeezing remains possible but challenging due to the weakness of the interaction, and has not been reported so far. Here, we measure the ponderomotively squeezed state of light scattered by a nanoparticle levitated in a free-space optical tweezer. We observe a reduction of the optical fluctuations by up to 25% below the vacuum level, in a bandwidth of about 15 kHz. Our results are explained well by a linearized dipole interaction between the nanoparticle and the electromagnetic continuum. These ponderomotive correlations open the door to quantum-enhanced sensing and metrology with levitated systems, such as force measurements below the standard quantum limit.

DOI: 10.1103/PhysRevLett.129.053602

Cavity-enhanced light-matter interaction is a central paradigm in condensed-matter physics [1], especially in the fields of cavity and circuit quantum electrodynamics [2,3]. More recently, researchers in cavity optomechanics have employed similar techniques in order to measure and control the motion of solid-state systems, from nanomechanical resonators to kilogram-scale mirrors [4].

Electromagnetic resonators also come with drawbacks, such as bandwidth limitations and reduced coupling efficiencies due to mode mismatching [5]. To circumvent these problems, there exist alternative coupling schemes that make use of traveling electromagnetic fields either in waveguides or directly in free space, rather than in cavities. In the context of optomechanics, these schemes have been studied with Brillouin and Raman scattering from bulk acoustic waves [6,7] and optical phonons [8,9], and in levitodynamics with optical tweezers [10–12].

The latter scenario is an example of a free-space system: here, an optical trap is formed for a dielectric nanoparticle by tightly focusing an intense laser field. The nanoparticle imprints a position-dependent phase to the scattered laser photons. Interferometric techniques allow one to retrieve this phase, effectively realizing a displacement measurement. At the same time, the nanoparticle recoils after a photon scattering event, which occurs at random times. This is a form of quantum backaction and generates fluctuations in the nanoparticle position. Recent experimental advances have made it possible to access a regime in which the quantum backaction is the dominant source of position fluctuations, which are efficiently recorded in phase measurements [13,14]. These advances enabled measurement-based ground-state cooling of the motional state of nanoparticles in free-space levitodynamics [15,16].

In addition to ground-state cooling, this quantum regime of measurement enables the generation of quantum correlations in the mode of the scattered light. The nanoparticle motion correlates the optical amplitude and phase quadratures, which are responsible for the quantum backaction and measurement imprecision, respectively. If strong enough, these correlations may lead to a reduction of the fluctuations of an optical quadrature below the level of vacuum fluctuations, a phenomenon known as ponderomotive squeezing [17,18]. In cavity optomechanics, this quantum squeezing has been observed with ultracold atoms [19], optomechanical photonic crystals [20], membrane resonators [21–23], and crystalline cantilevers [24]. All these experiments are based on a cavity-enhanced optomechanical interaction. To date, no observations of ponderomotive squeezing in free-space optomechanical systems have been reported.

In this work, we measure squeezing by 25% below the vacuum noise in the light scattered by a levitated nanoparticle in free space. We fully reconstruct the state of the squeezed optical mode by homodyne tomography [25–27]. Furthermore, we explain our experiments with quantum optics theory, which assumes a linearized dipole interaction between the nanoparticle motion and the electromagnetic field.

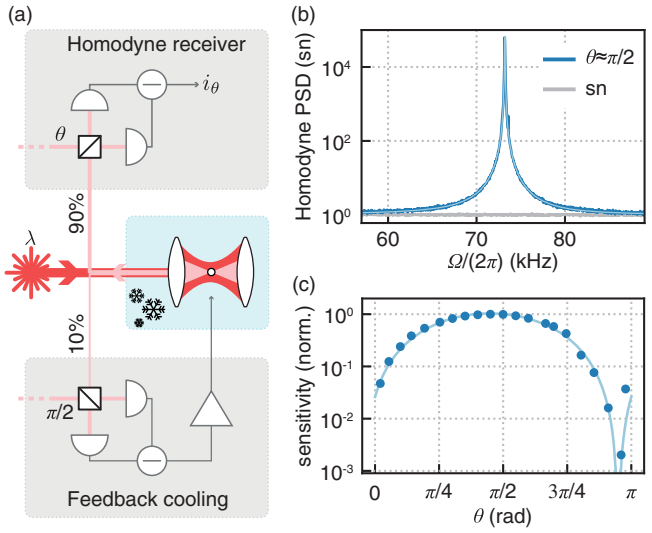

FIG. 1. Free-space levitated optomechanics. (a) Experimental setup. (b) Power spectral density (PSD) of a phase quadrature measurement, normalized to the shot-noise (sn) background. (c) Sensitivity to mechanical motion, normalized to its maximum. The sensitivity is measured as the detector response to an off-resonant sinusoidal force acting on the particle. The light blue line is a sinusoidal fit.

Our experimental setup is shown in Fig. 1(a) and consists of a spherical silica nanoparticle of 100 nm diameter trapped in the focus of an optical tweezer. The laser (wavelength 1550 nm, power 1.2 W) is linearly polarized along the x direction and propagates along the direction z. In the following, we will only consider the motion along this longitudinal direction (z axis). We form the optical tweezer by strongly focusing the laser by an aspheric lens that is located inside a 4 K cryostat. More details can be found in Ref. [16]. Once cooled down, the consequent cryogenic pumping mechanism evacuates the volume around the optical trap to a pressure below 10^{-9} mbar. At this pressure, the quantum backaction from the photon scattering dominates over the motional decoherence induced by collisions with the surrounding gas molecules [13]. We perform shot-noise limited homodyne detection to monitor the field scattered by the nanoparticle (scattered power $P_{\mathrm{sc}} \approx 2\ \mu$W), characterized by the amplitude and phase quadratures X_{out} and Y_{out}, respectively [16]. To do so, we overlap the scattered light with a strong coherent local oscillator beam (LO) with relative phase θ. We optimize the LO Gaussian transverse profile to match the one of the scattered light in the backward direction, such that the detection efficiency η_d of the longitudinal motion is maximized [28]. We model the losses and finite detection efficiency with a fictitious beam splitter of transmissivity η_d in front of the detector [29]. The homodyne photocurrent becomes $i_\theta = \sqrt{\eta_{\mathrm{d}}} X^\theta_{\mathrm{out}} + \sqrt{1-\eta_d} X_\nu$, where X_ν is the amplitude quadrature of an uncorrelated field in the vacuum state entering from the dark port of the fictitious beam splitter. In the equation for the photocurrent, we have introduced the rotated quadrature of the scattered field

$$X^\theta_{\mathrm{out}} = \cos(\theta) X_{\mathrm{out}} + \sin(\theta) Y_{\mathrm{out}}. \tag{1}$$

In the experiment, we split the scattered field in two parts, as shown in Fig. 1(a). A small fraction (10%) is used to perform a homodyne phase measurement to feedback-cool the particle motion [16]. The remaining part (90%) is sent to a different, out-of-loop homodyne receiver. This is the main detector of our experiments and we use it to measure ponderomotive squeezing. For this detector, we stabilize its LO phase, θ, to any value in the range $[0, \pi]$ to measure the corresponding optical quadrature [30].

In Fig. 1(b), we show the power spectral density (PSD) of the homodyne photocurrent, S^θ_{ii}, for a phase quadrature measurement ($\theta \approx \pi/2$) [47]. The flat noise floor in the spectrum arises from the vacuum noise of the probing light field. On top of this background stands a Lorentzian peak, which represents the nanoparticle motion. By fitting the PSD with a Lorentzian function, we extract the mechanical resonance frequency $\Omega_m/(2\pi) = 73.25$ kHz and the damping rate $\gamma_m/(2\pi) = 40$ Hz. This damping rate results from the mild feedback cooling exerted on the nanoparticle.

We now measure the PSD as we change the angle θ in the range $[0, \pi]$ [30]. This reduces the sensitivity of our measurements of the particle motion, which is solely contained in the phase quadrature Y_{out}. To characterize this sensitivity, we exert an off-resonant (90 kHz) sinusoidal force on the nanoparticle. We exert this force electrically, which is possible thanks to the net charge carried by the nanoparticle [16,48]. The driven motion appears in the homodyne photocurrent as a sinusoidal oscillation at 90 kHz. We record its amplitude for different angles θ, as shown in Fig. 1(c). The maximum (minimum) response is shifted from the phase (amplitude) quadrature at $\pi/2$ (π) by $\sim 0.05\pi$. This deviation is caused by an additional, weak reflection of the tweezer light copropagating backward with the scattered light toward the homodyne detector.

In Fig. 2, we compare two PSDs acquired close to the amplitude quadrature, at $\theta \approx 0$ (red) and at $\theta \approx 0.9\pi$ (green), with one at the phase quadrature $\theta \approx \pi/2$ (blue). The former two show an asymmetric Fano line shape rather than a Lorentzian one, suggesting interference between a broadband background, generated by both optical quadratures, and a resonant process, generated by the mechanical motion driven by the optical amplitude quadrature. The measured spectral noise lies below the shot noise within about 15 kHz bandwidth, with a maximum noise reduction of 25%. This is the manifestation of ponderomotive squeezing of the scattered light field [17,18].

The backscattered field contains infinitely many modes oscillating at every frequency Ω. Because experimentally we can only access time traces of finite length, we can

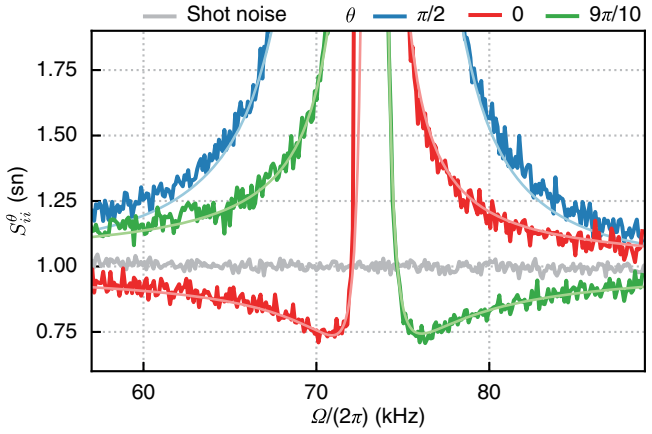

FIG. 2. Ponderomotive squeezing. Enlarged view of three different PSDs, at the phase quadrature (blue) and close to the amplitude one (red and green). The solid light-colored lines are the results of the fits to Eq. (5). The gray trace is the measured shot noise. We have subtracted from the PSDs a small classical noise contribution originating from the LO [30].

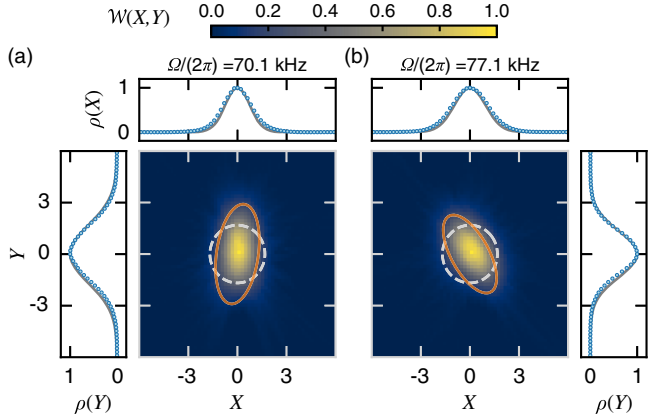

FIG. 3. Homodyne tomography of ponderomotively squeezed light. (a),(b) Reconstructed Wigner functions of modes centered at, respectively, $\Omega/(2\pi) = 70.1$ kHz and 77.1 kHz. The solid orange (dashed light gray) line indicates the covariance ellipse with 2 standard deviations of the squeezed (vacuum) state. Above and aside the Wigner functions we show the marginals distributions, ρ, for X and Y, respectively. Blue dots are data; the dark gray lines are theoretical predictions [30]. The optical quadratures are normalized such that the vacuum noise standard deviation is $1/\sqrt{2}$.

extract realizations of so-called "temporal modes" $r_{\theta,\Omega}$, defined as [49]

$$r_{\theta,\Omega} = \frac{1}{\sqrt{T}} \int_{-T/2}^{T/2} dt\, e^{i\Omega t} i_\theta(t), \tag{2}$$

which in the spectral domain corresponds to a frequency bin centered at Ω and with a width $1/T$. In our experiment, we choose $T \approx 8$ ms to be larger than the correlation time $1/\gamma_m$ in order to consider statistically independent realizations. Note that γ_m corresponds to the decay rate of "classical" correlations, as opposed to the much faster decay of quantum correlations due to decoherence. In order for the realizations of $r_{\theta,\Omega}$ to be independent, however, both classical and quantum correlations need to decay, hence our choice of the time window T. For each angle θ in the set shown in Fig. 1(c) and for each frequency Ω of interest, we extract realizations of the temporal mode in Eq. (2).

We collect an ensemble of $\sim 10^4$ realizations for both the real and imaginary part of $r_{\theta,\Omega}$, and then we compute their histograms. We repeat this procedure for different angles θ. The histograms correspond to marginals of the Wigner quasiprobability distribution $\mathcal{W}(X, Y)$ along the angle θ with respect to the X axis [26,50,51]. To reconstruct the function $\mathcal{W}(X, Y)$, we apply the inverse Radon transform to the set of histograms [30]. In Fig. 3, we show the experimentally reconstructed Wigner functions for two modes centered at $\Omega/(2\pi) = 70.1$ kHz in (a) and 77.1 kHz in (b), for which we have the strongest correlations. Since the optical states are Gaussian, the Wigner function is fully determined by the quadratures' means and covariance matrix. The latter can be simply estimated from three PSDs at different angles [30]. We apply this idea to estimate the covariance ellipses shown in Fig. 3. The covariance ellipse from the scattered light (solid orange line) is narrower than the one of the vacuum state (dashed light gray line) along some directions, a distinctive fingerprint of squeezing. We also notice that the angle of squeezing changes with the frequency Ω of the temporal mode. The minor axis of the covariance ellipse is rotated by $-8°$ with respect to the X axis for the mode at 70.1 kHz and by 30° for the one at 77.1 kHz.

Light squeezing via the motion of a mechanical system induced by quantum backaction is known as ponderomotive squeezing, a phenomenon that has been recently observed in optomechanics [19–24]. Therein, the squeezed optical mode is determined by the cavity resonance driven by the laser and interacting with the mechanical oscillator. In contrast, in our case the nanoparticle simultaneously interacts with all the modes of the electromagnetic continuum due to the absence of a cavity. We analyze our experiments with a theoretical framework, which assumes a linearized dipolar light-matter interaction [15,52–55]. The longitudinal nanoparticle motion interacts with a set of plane waves of the electromagnetic field (similarly for the motion along other directions). This combination defines a distinct optical mode, the amplitude and phase quadratures of which we label $X_{\rm in}$ and $Y_{\rm in}$ [30]. The spatial distribution of this mode, which we term "interacting mode," has been first derived in Ref. [28], where it played the role of information density patterns in an optimal position measurement of a dipolar scatterer.

With the use of the interacting mode and in the interaction picture with respect to the free field, the interaction Hamiltonian of our system is $H_{\rm int} = -\sqrt{4\Gamma_{\rm qba}} X_{\rm in} q$, where $\Gamma_{\rm qba}$ is a rate characterizing the interaction strength, and q is

the position operator normalized to $\sqrt{\hbar/(m\Omega_m)}$, with m the nanoparticle mass. After including the harmonic potential generated by the optical tweezer, the Heisenberg equation of motion for q becomes

$$\ddot{q} + \Omega_m^2 q + \gamma_m \dot{q} = \Omega_m[\xi(t) + \sqrt{4\Gamma_{\mathrm{qba}}} X_{\mathrm{in}}(t)], \quad (3)$$

where we introduced the damping rate γ_m that accounts for the surrounding gas and for the feedback cooling. The term ξ is a white thermal force that satisfies the correlation $\langle\overline{\xi(t)\xi(t')}\rangle = 2\gamma_m(\bar{n} + 1/2)\delta(t - t')$, where $\bar{n}$ is the average phonon occupancy [56,57]. The last term in Eq. (3) is the quantum backaction exerted on the particle by the interacting mode. At the same time, the nanoparticle motion affects the quadratures (X_{in}, Y_{in}) of the interacting modes. The resulting quadratures (X_{out}, Y_{out}), labeled output, are derived from the input-output relations [58]

$$X_{\mathrm{out}}(t) = X_{\mathrm{in}}(t), \quad (4a)$$

$$Y_{\mathrm{out}}(t) = Y_{\mathrm{in}}(t) + \sqrt{4\Gamma_{\mathrm{qba}}} q(t). \quad (4b)$$

The output quadratures of Eq. (4) are the quantities that we measure in our experiments and that appear in Eq. (1). From Eqs. (3) and (4), we calculate the following PSD for the homodyne photocurrent:

$$S_{ii}^{\theta}(\Omega) = 1 + S_{\mathrm{imp},\theta}^{-1} |\chi(\Omega)|^2 S_{FF}^{\mathrm{tot}} + 2S_{\mathrm{c}}^{\theta}(\Omega), \quad (5)$$

where we normalized the spectrum to the background noise $S_{\mathrm{imp},\theta}$ (first term on the right-hand side). The second term arises from the mechanical displacement, with the susceptibility $\chi(\Omega) = \Omega_m/(\Omega_m^2 - \Omega^2 - i\gamma_m\Omega)$ and the total force spectrum $S_{FF}^{\mathrm{tot}} = 2[\Gamma_{\mathrm{qba}} + \gamma_m(\bar{n} + 1/2)]$. The sensitivity to the motion is represented by $S_{\mathrm{imp},\theta}^{-1} = 8\eta_d\Gamma_{\mathrm{qba}}\sin^2(\theta)$, which is shown in Fig. 1(c). Finally, the last term in Eq. (5) represents the frequency-dependent correlations between the background and the displacement noise $S_c^{\theta}(\Omega) = 2\eta_d\Gamma_{\mathrm{qba}}\mathrm{Re}[\chi(\Omega)]\sin(2\theta)$. These correlations are responsible for the asymmetric line shape in Fig. 2 and for the frequency-dependent squeezing angle in Fig. 3.

The figure of merit for the degree of ponderomotive squeezing is the measurement efficiency $\eta_{\mathrm{meas}} = \Gamma_{\mathrm{meas}}/\Gamma_{\mathrm{tot}}$, where we have introduced for convenience the total decoherence rate $\Gamma_{\mathrm{tot}} = \Gamma_{\mathrm{qba}} + \gamma_m(\bar{n} + 1/2)$ and the measurement rate $\Gamma_{\mathrm{meas}} = \eta_d\Gamma_{\mathrm{qba}}$. The correlations lead to significant ponderomotive squeezing when the measurement rate approaches the total decoherence rate, that is $\eta_{\mathrm{meas}} \sim 1$. In this limit, the minimum value of the spectrum approaches $S_{ii}^{\theta} \approx 1 - \eta_{\mathrm{meas}}$ close to the resonance frequency [22]. We use Eq. (5) to simultaneously fit all the measured spectra, some of which are shown in Fig. 2 [30]. We extract the rates $\Gamma_{\mathrm{tot}}/(2\pi) = 5.0$ kHz and $\Gamma_{\mathrm{meas}}/(2\pi) = 1.4$ kHz, yielding a measurement efficiency of $\eta_{\mathrm{meas}} = 0.28$. These results are consistent with what we previously reported in Ref. [16]. These rates allow us to calibrate the displacement measurements in units of zero-point motion. This calibration technique relies only on the ponderomotive correlations present in the spectra. These spectra, in turn, are calibrated against the optical shot noise, which is easy to quantify experimentally. The estimated parameters can be also used to compute the theoretical Wigner functions for the modes at $\Omega/(2\pi) = 70.1$ kHz and 77.1 kHz, whose X and Y marginals are shown in Fig. 3. Both the fits of the spectra and the marginals extracted from the theoretical Wigner functions are in good agreement with the measurements.

We have experimentally observed squeezing of light scattered by a levitated nanoparticle and we have fully characterized the optical state with homodyne tomography. We have measured a reduction of the optical quantum fluctuations by 25%, which is due to the large measurement efficiency featured by our system. Notably, we observe ponderomotive squeezing from a single particle in free space, without the need of an optical resonator to enhance the optomechanical coupling. We model our experiments by using a linearized dipolar treatment of the light-matter interaction.

The ponderomotive correlations present in the scattered field can be readily exploited to provide quantum enhancements in force sensing applications [59], such as gravitational wave detectors based on levitated sensors [60], in testing fundamental force laws [61], and in the search for dark matter [62].

This research was supported by the Swiss National Science Foundation (SNF) through the NCCR-QSIT program (Grant No. 51NF40-160591), by the European Union's Horizon 2020 research and innovation program under Grants No. 863132 (iQLev) and 951234 (Q-Xtreme). We thank M. L. Mattana for her contributions to the experimental setup.

A. M. and M. R. contributed equally to this work.

Note added.—We recently became aware of a related independent work by Magrini *et al.* [63].

*Present address: Department of Physics, Humboldt-Universität zu Berlin, 10099 Berlin, Germany.

[1] F. J. Garcia-Vidal, C. Ciuti, and T. W. Ebbesen, Science **373**, eabd0336 (2021).
[2] *Cavity Quantum Electrodynamics*, edited by P. R. Berman (Academic Press, Boston, 1994).
[3] A. Blais, A. L. Grimsmo, S. M. Girvin, and A. Wallraff, Rev. Mod. Phys. **93**, 025005 (2021).
[4] M. Aspelmeyer, T. J. Kippenberg, and F. Marquardt, Rev. Mod. Phys. **86**, 1391 (2014).

[5] D. Roy, C. M. Wilson, and O. Firstenberg, Rev. Mod. Phys. **89**, 021001 (2017).

[6] W. H. Renninger, P. Kharel, R. O. Behunin, and P. T. Rakich, Nat. Phys. **14**, 601 (2018).

[7] N. T. Otterstrom, R. O. Behunin, E. A. Kittlaus, and P. T. Rakich, Phys. Rev. X **8**, 041034 (2018).

[8] K. C. Lee, M. R. Sprague, B. J. Sussman, J. Nunn, N. K. Langford, X.-M. Jin, T. Champion, P. Michelberger, K. F. Reim, D. England, D. Jaksch, and I. A. Walmsley, Science **334**, 1253 (2011).

[9] M. D. Anderson, S. Tarrago Velez, K. Seibold, H. Flayac, V. Savona, N. Sangouard, and C. Galland, Phys. Rev. Lett. **120**, 233601 (2018).

[10] A. Ashkin and J. M. Dziedzic, Appl. Phys. Lett. **28**, 333 (1976).

[11] K. G. Libbrecht and E. D. Black, Phys. Lett. A **321**, 99 (2004).

[12] C. Gonzalez-Ballestero, M. Aspelmeyer, L. Novotny, R. Quidant, and O. Romero-Isart, Science **374**, eabg3027 (2021).

[13] V. Jain, J. Gieseler, C. Moritz, C. Dellago, R. Quidant, and L. Novotny, Phys. Rev. Lett. **116**, 243601 (2016).

[14] F. Tebbenjohanns, M. Frimmer, V. Jain, D. Windey, and L. Novotny, Phys. Rev. Lett. **124**, 013603 (2020).

[15] L. Magrini, P. Rosenzweig, C. Bach, A. Deutschmann-Olek, S. G. Hofer, S. Hong, N. Kiesel, A. Kugi, and M. Aspelmeyer, Nature (London) **595**, 373 (2021).

[16] F. Tebbenjohanns, M. L. Mattana, M. Rossi, M. Frimmer, and L. Novotny, Nature (London) **595**, 378 (2021).

[17] C. Fabre, M. Pinard, S. Bourzeix, A. Heidmann, E. Giacobino, and S. Reynaud, Phys. Rev. A **49**, 1337 (1994).

[18] S. Mancini and P. Tombesi, Phys. Rev. A **49**, 4055 (1994).

[19] D. W. C. Brooks, T. Botter, S. Schreppler, T. P. Purdy, N. Brahms, and D. M. Stamper-Kurn, Nature (London) **488**, 476 (2012).

[20] A. H. Safavi-Naeini, S. Gröblacher, J. T. Hill, J. Chan, M. Aspelmeyer, and O. Painter, Nature (London) **500**, 185 (2013).

[21] T. P. Purdy, P.-L. Yu, R. W. Peterson, N. S. Kampel, and C. A. Regal, Phys. Rev. X **3**, 031012 (2013).

[22] W. H. P. Nielsen, Y. Tsaturyan, C. B. Møller, E. S. Polzik, and A. Schliesser, Proc. Natl. Acad. Sci. U.S.A. **114**, 62 (2017).

[23] J. Chen, M. Rossi, D. Mason, and A. Schliesser, Nat. Commun. **11**, 943 (2020).

[24] N. Aggarwal, T. J. Cullen, J. Cripe, G. D. Cole, R. Lanza, A. Libson, D. Follman, P. Heu, T. Corbitt, and N. Mavalvala, Nat. Phys. **16**, 784 (2020).

[25] K. Vogel and H. Risken, Phys. Rev. A **40**, 2847 (1989).

[26] D. T. Smithey, M. Beck, M. G. Raymer, and A. Faridani, Phys. Rev. Lett. **70**, 1244 (1993).

[27] A. I. Lvovsky, H. Hansen, T. Aichele, O. Benson, J. Mlynek, and S. Schiller, Phys. Rev. Lett. **87**, 050402 (2001).

[28] F. Tebbenjohanns, M. Frimmer, and L. Novotny, Phys. Rev. A **100**, 043821 (2019).

[29] H. Yuen and J. Shapiro, IEEE Trans. Inf. Theory **26**, 78 (1980).

[30] See Supplemental Material at http://link.aps.org/supplemental/10.1103/PhysRevLett.129.053602, which includes Refs. [31–46], for the derivation of the free-space quantum Langevin equations of the levitated nanoparticle, and for additional experimental details.

[31] P. Maurer, C. Gonzalez-Ballestero, and O. Romero-Isart, arXiv:2106.07975.

[32] F. Ricci, R. A. Rica, M. Spasenović, J. Gieseler, L. Rondin, L. Novotny, and R. Quidant, Nat. Commun. **8**, 15141 (2017).

[33] F. Tebbenjohanns, M. Frimmer, A. Militaru, V. Jain, and L. Novotny, Phys. Rev. Lett. **122**, 223601 (2019).

[34] E. Hebestreit, M. Frimmer, R. Reimann, and L. Novotny, Phys. Rev. Lett. **121**, 063602 (2018).

[35] T. M. Hoang, R. Pan, J. Ahn, J. Bang, H. T. Quan, and T. Li, Phys. Rev. Lett. **120**, 080602 (2018).

[36] L. Novotny, Phys. Rev. A **96**, 032108 (2017).

[37] A. C. Pflanzer, O. Romero-Isart, and J. I. Cirac, Phys. Rev. A **86**, 013802 (2012).

[38] A. A. Clerk, M. H. Devoret, S. M. Girvin, F. Marquardt, and R. J. Schoelkopf, Rev. Mod. Phys. **82**, 1155 (2010).

[39] K. Børkje, A. Nunnenkamp, B. M. Zwickl, C. Yang, J. G. E. Harris, and S. M. Girvin, Phys. Rev. A **82**, 013818 (2010).

[40] V. Sudhir, D. J. Wilson, R. Schilling, H. Schütz, S. A. Fedorov, A. H. Ghadimi, A. Nunnenkamp, and T. J. Kippenberg, Phys. Rev. X **7**, 011001 (2017).

[41] K. Jacobs and D. A. Steck, Contemp. Phys. **47**, 279 (2006).

[42] H. M. Wiseman and G. J. Milburn, *Quantum Measurement and Control* (Cambridge University Press, Cambridge, England, 2010).

[43] V. B. Braginsky and F. Y. Khalili, *Quantum Measurement* (Cambridge University Press, Cambridge, England, 1992).

[44] *Cavity Optomechanics*, edited by M. Aspelmeyer, T. J. Kippenberg, and F. Marquardt (Springer, Berlin, Heidelberg, 2014).

[45] A. H. Andersen and A. C. Kak, Ultrasonic Imaging **6**, 81 (1984).

[46] S. Van Der Walt, J. L. Schönberger, J. Nunez-Iglesias, F. Boulogne, J. D. Warner, N. Yager, E. Gouillart, and T. Yu, PeerJ **2**, e453 (2014).

[47] We adopt the following definition $S_{ii}^{\theta}(\Omega) = 1/(2\pi)\int_{\boldsymbol{R}} d\tau\, e^{i\Omega\tau}\overline{\langle i_\theta(t) i_\theta(t+\tau)\rangle}$, where the overline indicates a symmetrized quantity.

[48] M. Frimmer, K. Luszcz, S. Ferreiro, V. Jain, E. Hebestreit, and L. Novotny, Phys. Rev. A **95**, 061801(R) (2017).

[49] S. Zippilli, G. Di Giuseppe, and D. Vitali, New J. Phys. **17**, 043025 (2015).

[50] G. Breitenbach, S. Schiller, and J. Mlynek, Nature (London) **387**, 471 (1997).

[51] A. I. Lvovsky and M. G. Raymer, Rev. Mod. Phys. **81**, 299 (2009).

[52] D. E. Chang, C. A. Regal, S. B. Papp, D. J. Wilson, J. Ye, O. Painter, H. J. Kimble, and P. Zoller, Proc. Natl. Acad. Sci. U.S.A. **107**, 1005 (2010).

[53] O. Romero-Isart, A. C. Pflanzer, M. L. Juan, R. Quidant, N. Kiesel, M. Aspelmeyer, and J. I. Cirac, Phys. Rev. A **83**, 013803 (2011).

[54] B. Rodenburg, L. P. Neukirch, A. N. Vamivakas, and M. Bhattacharya, Optica **3**, 318 (2016).

[55] C. Gonzalez-Ballestero, P. Maurer, D. Windey, L. Novotny, R. Reimann, and O. Romero-Isart, Phys. Rev. A **100**, 013805 (2019).

[56] V. Giovannetti and D. Vitali, Phys. Rev. A **63**, 023812 (2001).
[57] The notation $\langle \overline{\xi(t)\xi(t')} \rangle$ refers to a symmetrized average, i.e., $\langle \xi(t)\xi(t') + \xi(t')\xi(t) \rangle / 2$.
[58] C. W. Gardiner and M. J. Collett, Phys. Rev. A **31**, 3761 (1985).
[59] D. Mason, J. Chen, M. Rossi, Y. Tsaturyan, and A. Schliesser, Nat. Phys. **15**, 745 (2019).
[60] A. Arvanitaki and A. A. Geraci, Phys. Rev. Lett. **110**, 071105 (2013).
[61] D. C. Moore and A. A. Geraci, Quantum Sci. Technol. **6**, 014008 (2021).
[62] D. Carney *et al.*, Quantum Sci. Technol. **6**, 024002 (2021).
[63] L. Magrini *et al.*, preceding Letter, Phys. Rev. Lett. **129**, 053601 (2022).